Received: 28 February 2023 | Revised: 15 June 2023 | Accepted: 7 July 2023

IET Radar, Sonar & Navigation

DOI: 10.1049/rsn2.12438

The Institution of Engineering and Technology WILEY

ORIGINAL RESEARCH

Maritime moving target detection and localisation technique for Global Navigation Satellite Signals-based passive multistatic radar

Ilaria Nasso | **Fabrizio Santi**

Department of Information Engineering Electronics and Telecommunications, Sapienza University of Rome, Rome, Italy

Correspondence
Ilaria Nasso.
Email: ilaria.nasso@uniroma1.it

Abstract

This article puts forward a ship target detection and localisation technique for GNSS-based passive multistatic radar. The approach capitalises on the large spatial diversity offered by navigation satellite constellations to provide maritime awareness using short integration time windows, thus bypassing the shortcomings suffered by approaches relying on long dwells typically considered in satellite-based passive radar systems. The proposed approach entirely operates on the Cartesian plane and it is able to provide in a single stage the detection and localisation of the target in the surveyed area. Theoretical and simulated performance analysis are provided to illustrate as the proposed approach can outperform conventional two-stages (i.e. bistatic detection then localisation) procedures, with particular regard to the case of significant radar cross section scintillation, likely experienced in the system under consideration. The effectiveness of the approach has been verified via experimental data acquired in a few scenarios of interest comprising opportunistic targets belonging to different types.

KEYWORDS

multistatic radar, passive radar, radar detection, radar localisation

1 | INTRODUCTION

Passive radar systems based on satellite transmissions are emerging as a promising option for maritime surveillance applications. With respect to conventional active radar systems, the sensors operate without a transmitting segment, thus not requiring dedicated spectrum resources and lowering the size, weight, and power consumption. These factors, along with the reduced electromagnetic pollution produced, facilitate their deployment in critical areas such as marine protected sites. Relying on transmissions from the space, the systems can work even in remote areas far from land such as economic exclusive zone or international waters, where the coverage of terrestrial illuminators such as DVB-T or FM radio base-stations cannot be guaranteed. Suitable illuminators of opportunity are communication satellites such as Iridium and Inmarsat [1–3], digital television satellites such as Astra and Eutelsat [4], and navigation satellites such as GPS and Galileo [5]. It is expected that the continuous update of the current missions and the advent of mega-constellations in LEO orbits, such as Starlink and OneWeb [6] will offer increasing possibilities for satellite-based passive radar technology in the next years.

Among the possible options, Global Navigation Satellite Signals (GNSS) represent a prospective solution. First, the design of these constellations guarantees a global, reliable and persistent coverage, noticeably with an a priori known signal structure which is the same worldwide, enabling the use of the same receiving system everywhere, without the need to adapt to local standards. Noticeably, GNSS provide transmitter redundancy with large spatial diversity, with relatively wide bandwidths (up to 10.23 MHz) and transmissions over multiple channels in the L-band. On the other hand, GNSS-based passive radar systems suffer for the limited power budget, making low the target observability in turn limiting the radar range [7].

The general trend to overcome such limitation is extending the integration time and over the last years a few techniques

have been conceived and developed for such a goal [7–15]. All these methods implement some kind of target motion compensation to correctly accumulate the received power over the long dwell considered (typically in the order of few tens of seconds). These methods have been proved to be a viable and effective solution to enhance the ship detection performance of the system. However, with respect to the standard short-time detection approaches, long-time integrations bring with them some relevant issues. The classical approach for moving target detection in passive radar is the Doppler filtering, requiring to apply to the range-compressed data a single bank of Doppler filters according to the possible target velocities. In contrast, when the integration time gets longer, both range and Doppler migration appears and must be corrected, requiring to add additional search variables to the detection space according to hypothesised motion model, increasing the computational complexity and memory usage. The situation is even worse in the case of maneuvering targets: losses are likely experienced if higher-order terms of the motions are neglected, but further expanding the search space become impractical because of the increased system complexity.

It is worth to point out that in GNSS-based passive radar a single receiver can collect the signals coming from multiple satellites, thus forming a multistatic passive radar system. This offers the nice possibility to localise the ship without resorting to expensive array receiver configurations: typically, the target is detected on the individual bistatic channels (i.e. satellites) and, in a successive stage, the detections are fused across bistatic pairs (typically by determining the intersections of bistatic ellipsoids) to localise it in Cartesian space [16, 17]. However, it is worth to point out that in the considered scenario the ships are illuminated by satellites that can be considerably separated in angles, in both the horizontal and vertical planes. Therefore, the bistatic radar cross section (RCS) may considerably fluctuate among the different channels: if the bistatic RCS experienced over one particular channel does not suffice to detect the ship, the use of that link for the localisation task is prevented.

In this work, expanding the preliminary results anticipated in ref. [18], we propose an approach able to combine the multistatic data in a common reference plane independent of the particular bistatic geometry. This potentially allows to achieve superior performance in both detection and localisation than conventional two stages (i.e. bistatic detections then localisation) procedures, as the receiver jointly processes unthresholded signals fully capitalising on the available information [12, 19, 20]. Particularly, the proposed approach projects the bistatic range and Doppler (RD) maps obtained over short-time intervals in a Cartesian plane representing the surveyed area. As such a plane is independent of the satellites' viewing angles, a direct integration over the available bistatic channels can be performed, reinforcing the target power and at the same time providing its Cartesian position. This approach is a modified version of the local-plane based technique originally proposed for bistatic [7] and multistatic [15] long-integration times procedures. Here, in contrast, the main goal is to trade the long-integration times with the spatial diversity offered by navigation satellites, in order to overcome the shortcomings suffered by migration compensation procedures over long datastreams. Capitalising on the RCS diversity experienced over multiple bistatic geometries, the method can provide an aggregate SNR potentially much higher than the one achievable in the individual bistatic systems attempting to increase the SNR extending the dwell time, especially in those scenarios where a large span of satellite-target-receiver orientations is observed.

Theoretical formulations are provided to illustrate the potential enhancements in target detection and localisation with respect to conventional two-stages procedures, considering the scintillation of the bistatic RCS with the different bistatic geometries. Numerical results for a number of use cases are provided in order to assess the maritime awareness performance of the proposed approach. Experimental results with Galileo satellites obtained in different scenarios and involving ship targets belonging to different classes are also provided, showing the wide applicability of the method in a number of operative conditions of practical interest for the GNSS-based passive radar technology.

The remainder of the paper is organised as follows: Section 2 details the operative conditions and the proposed technique, while Section 3 provides theoretical and simulated performance analysis; experimental results are then shown in Section 4 and Section 5 closes the paper.

2 | GNSS-BASED MULTISTATIC RADAR FOR MARITIME SURVEILLANCE

We consider a single receiving-only device observing remotely the maritime area of interest. This receiver could be mounted on the land for applications such as coastal surveillance or support to port operations, or it could be installed on a moored buoy, for example, for offshore trade route control. The receiver is equipped with two RF channels, one for reference and one for surveillance. The former uses a low-gain antenna pointed towards the sky to register the direct signals, while the latter collects the reflected signals from the surveyed area via a higher-gain antenna. As navigation satellites are designed to guarantee multiple satellites simultaneously in visibility from every point of the Earth surface (4–8 for a single constellation, so that over 30 satellites could be available considering all the global constellations in full capacity), multiple bistatic links can be set. Indeed, as GNSS operate with code/frequency division multiple access schemes, the signals from different satellites can be straightforwardly separated and individually processed.

Let N be the number of satellites acquired by the receiver and, as sketched in Figure 1, let us define a $(0, X, Y, Z)$ Cartesian reference system centred in the receiver position. Without loss of generality, the X-axis denotes the surveillance channel antenna steering direction. The $Z = 0$ plane represents the maritime area to survey, and we assume on it a ship target located in position $\boldsymbol{p} = [x, y, 0]^T$, which must be detected and localised. To achieve such goals with the system under consideration, three main steps are usually implemented as

detailed below and shown in Figure 2. Steps 1 and 2 are separately implemented for each bistatic channel (bistatic processing), while step 3 concerns multistatic data combination, typically implemented as sketched in the upper branch on Figure 2. As GNSS signals are transmitted continuously, a preliminary pulsed radar reformatting is implemented by defining an equivalent pulse repetition interval (PRI), typically set equal to the length of the pseudo random noise (PRN) sequence of the transmissions (1 ms).

1) Signal synchronisation – In passive radar systems, cross-correlation between direct and reflected path data is implemented to mimic the matched filtering and compress the radar data. However, because of the power budget restrictions, in the GNSS-based case a noise free replica of the direct signal must be retrieved. This is obtained by tracking the direct signal parameters (i.e. time delay, Doppler, phase, and, if one exists, navigation message) and exploiting the knowledge of the PRN codes [5].
2) Range and Doppler (RD) processor – After range compression, Doppler filtering over a coherent processing interval (CPI) of duration T_a is implemented to achieve an RD map. T_a is usually kept limited at 2–3 s so that ship complex reflectivity can be assumed constant [5]. Moreover, as analysed in [7], range and Doppler cell migration effects within such time intervals could be neglected considering the relatively coarse range resolution and the limited velocity of the ship targets. Therefore, the RD map $\mathcal{B}_i$ pertaining the i th bistatic channel can be obtained via a slow-time FFT. Decision threshold methods are then applied after square modulus extraction to detect the target.
3) Bistatic ranges intersection – The target position in the local plane can be then obtained by multilateration approaches, consisting in intersecting the bistatic iso-ranges pertaining the $\overline{N} \leq N$ bistatic channels where target detection occurred [16, 17].

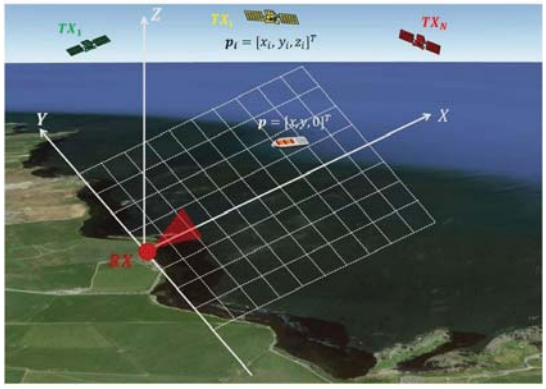

FIGURE 1 System geometry.

As discussed in the introduction, the restricted power budget provided by GNSS may make ineffective the method above because the high probability of missed detections, in turn worsening the localisation capability, which is completely prevented if $\overline{N}$ is lower than a minimum number (i.e. 2 for localisation on the ground plane). To reinforce the target power at each bistatic channel, RD processor is often modified to operate with longer dwells. Typically, multi-frame integration procedures are implemented, performing a quadratic integration of the maps pertaining consecutive frames. However, these methods require compensating the target motion among the different frames by resorting to proper banks based on assumed motion model, and being each branch of the bank matched to a specific set of model parameters [7]. Therefore, significant losses may be experienced if the actual target motion sensibly deviates from the assumed model. Moreover, the hard decision made at each bistatic channel prevents the exploitation of those channels where missed detection occurred anyway, for example, because of a small bistatic RCS.

To overcome such drawbacks, the proposed procedure modifies the conventional approach as follows and as depicted in the lower branch of Figure 2. Particularly, bistatic RD processors still operate on short CPI, but in lieu of peripheral decisions, a combination of the unthresholded multistatic data is implemented. Therefore, the extra gain typically obtained by multi-frame procedures can be achieved with short dwells by exploiting the available spatial diversity, at the same time using all the available information for the localisation task.

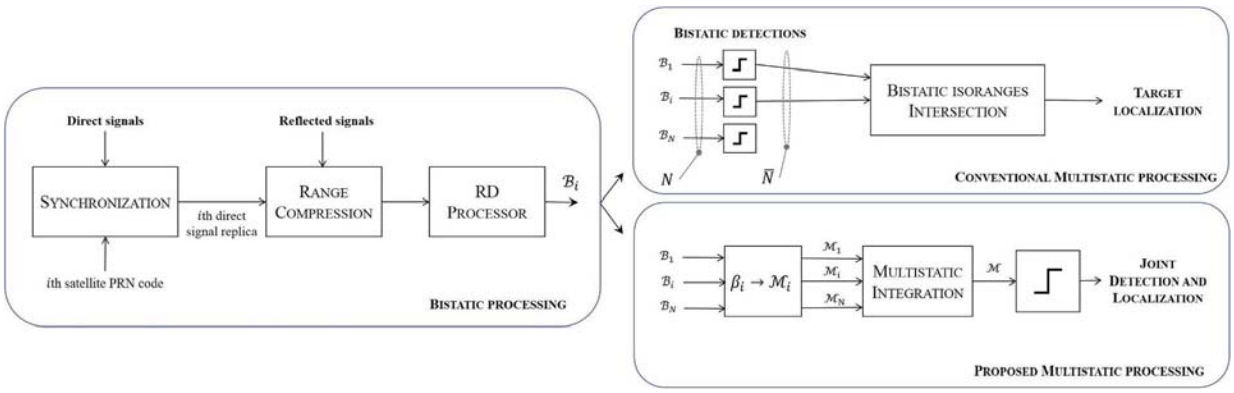

FIGURE 2 Bistatic and multistatic processing schemes.

In the system under consideration, the target range position in the map $\mathcal{B}_i$ is equal to

$$r_i = \left\|\boldsymbol{p}_i - \boldsymbol{p}\right\| + \left\|\boldsymbol{p}\right\| - \left\|\boldsymbol{p}_i\right\| \tag{1}$$

where $\boldsymbol{p}_i$ denotes the i th satellite position and $\| * \|$ is the Euclidian norm, while the Doppler position is given by

$$f_i = -\frac{1}{\lambda}\left(\frac{(\boldsymbol{p}_i^T - \boldsymbol{p}^T)(\boldsymbol{v}_i - \boldsymbol{v})}{\left\|\boldsymbol{p}_i - \boldsymbol{p}\right\|} + \frac{\boldsymbol{p}^T\boldsymbol{v}}{\left\|\boldsymbol{p}\right\|} - \frac{\boldsymbol{p}_i^T\boldsymbol{v}_i}{\left\|\boldsymbol{p}_i\right\|}\right) \tag{2}$$

where λ is the wavelength (for sake of simplicity, we assume the N transmitters sharing the same carrier frequency, but the approach can be easily extended to the multi-frequency case), and $\boldsymbol{v}_i$ and $\boldsymbol{v}$ are the satellite and target velocity vectors respectively.

It is worth to point out that, in the equations above, the satellite position and velocity are known quantity. Indeed, these information can be extracted by demodulating the navigation messages broadcasted by the satellite in real time. Therefore, for a given target velocity $\boldsymbol{v}_b$, from $\mathcal{B}_i$ a Cartesian map $\mathcal{M}_i$ can be obtained by selecting the i th RD cell corresponding to each position $\boldsymbol{p}$ of the surveyed area. Namely, a stack of Cartesian maps $\mathcal{M}_i(x, y; \boldsymbol{v}_b)$ for a suitable set of hypothesised target velocity is obtained. As bistatic data have been projected in a common domain independent of the i th bistatic geometry, a direct data integration on a pixel basis can be realised, that is,

$$\mathcal{M}(x, y; \boldsymbol{v}_b) = \frac{1}{N}\sum\nolimits_{i=1}^{N} |\mathcal{M}_i(x, y; \boldsymbol{v}_b)|^2 \tag{3}$$

Threshold detection is then applied to each map in the stack. It is worth to point out that, unlike the conventional scheme where $\overline{N}$ channels only are exploited, in this type of multistatic data fusion all the available channels contribute to the final decisions. The maximum integration gain is obtained in the map in the stack corresponding to the velocity closest to the actual value. In such a map, the best alignment of the target energy among the $\mathcal{M}_i$ maps is indeed achieved in correspondence of the target actual location, thus providing in a single stage target detection and localisation.

Of course, the computational complexity of the proposed approach is higher than conventional bistatic detections then localisation procedure, as the projection of the bistatic $\mathcal{B}_i$ maps into the Cartesian maps $\mathcal{M}_i(x, y; \boldsymbol{v}_b)$ requires the computation of N_p points defining the surveyed area. Sampling of the Cartesian grid could be set by imposing a bin spacing equal to the best range and azimuth resolution provided by the system [7]. Therefore, the computational complexity of the technique increases linearly with the number of satellites. However, it is worth to stress that in the considered system configuration, the same receiving station acts as a collector of the multistatic data. Therefore, regardless the number of involved satellites, all the data can be locally processed with no need to configure a broadband communication channel among the nodes of the multistatic radar configuration, which is often a fundamental bottleneck for implementing unthresholded data combinations in distributed systems.

3 | PERFORMANCE ANALYSIS

In this section, the performance of the conventional and proposed processing schemes are theoretically derived and then compared via numerical analysis.

3.1 | Theoretical performance

Let $\mathscr{k}_i$ be the cell under test of the map $\mathcal{B}_i$ and let us formulate a binary hypothesis test as

$$\mathscr{k}_i = \begin{cases} w & ,\mathcal{H}_0 \\ A_i + w & ,\mathcal{H}_1 \end{cases} \tag{4}$$

Under the null hypothesis $\mathcal{H}_0$, the cell contains disturbance only, denoted as w. As the system is essentially noise limited [7], w can be modelled as a white Gaussian noise with power $\mathrm{P_w}$, that is, $w \sim \mathcal{CN}(0, \mathrm{P_w})$ (being $\mathcal{CN}$ the complex normal). As the considered configuration comprises a single receiver, the same noise mean power level is experienced by all the bistatic channels. Under the alternative hypothesis $\mathcal{H}_1$, $\mathscr{k}_i$ is composed by signal plus noise, A_i denoting the signal complex amplitude, which can be modelled as a zero-mean complex normal random variable with variance α_i^2, that is, $A_i \sim \mathcal{CN}\left(0, \alpha_i^2\right)$. Namely, α_i^2 represents the target mean power as viewed by the i th bistatic channel: considering the scintillation of the target RCS with the illumination angle, this parameter is assumed to vary with the bistatic geometry.

In the conventional processing, individual decisions are taken at each channel. From Equation (4), the probability of false alarm pertaining the i th baseline is given by

$$P_{\mathrm{FA}_i}^{\mathscr{k}} = e^{-\eta_i^{\mathscr{k}}/P_w} \tag{5}$$

where $\eta_i^{\mathscr{k}}$ is the threshold. Typically, the same probability of false alarm is set in all the bistatic channels. Therefore, we can set $\eta_i^{\mathscr{k}} = \eta^{\mathscr{k}}$ and $P_{\mathrm{FA}_i}^{\mathscr{k}} = P_{FA}^{\mathscr{k}}\ \forall\, i$.

Let $SNR_i = \alpha_i^2/\mathrm{P_w}$ be the signal-to-noise ratio (SNR) pertaining the i th channel. The corresponding probability of detection is equal to

$$P_{D_i}^{\mathscr{k}} = e^{-\frac{\eta^{\mathscr{k}}/P_w}{SNR_i+1}} \tag{6}$$

After thresholding, $\overline{N} \le N$ bistatic detections are available and the corresponding ranges are intersected via multilateration methods. Localisation is enabled if at least $N_{min} = 2$ detections occur ($N_{min} = 3$ in case of localisation in 3D). The localisation probability is then equal to the probability that $\overline{N} \in [N_{min}, N]$. Since the bistatic RD maps represent independent statistic

events characterised by generally different probabilities of detection, this can be computed as a cumulative Poisson binomial distribution of independent Bernoulli trials with different probabilities [21]

$$P_L^{\boldsymbol{\ell}} = \sum_{l=N_{min}}^{N} \sum_{\mathcal{A}\in\mathcal{F}_l} \prod_{i\in\mathcal{A}} P_{D_i}^{\boldsymbol{\ell}} \prod_{j\in\mathcal{A}^C} \left(1 - P_{D_j}^{\boldsymbol{\ell}}\right) \tag{7}$$

where $\mathcal{F}_l$ is the set of all the subsets of l integers that can be selected from $\{N_{min}, \ldots, N\}$ (e.g. for $N = 3$ and $N_{min} = 2$, $\mathcal{F}_2 = \{(1,2),(1,3),(2,3)\}$), $\mathcal{A}$ represents the subsets of $\mathcal{F}_l$, $\mathcal{A}^C$ the complement of $\mathcal{A}$ ($\mathcal{A}^C = \{N_{min}, \ldots, N\}\backslash\mathcal{A}$). In the special case that the same SNR is experienced by all the bistatic channels, $P_{D_i}^{\boldsymbol{\ell}} = P_D^{\boldsymbol{\ell}}\ \forall\, i$ and (9) simplifies to

$$P_L^{\boldsymbol{\ell}} = \sum_{j=N_{min}}^{N} \binom{N}{j} \left(P_D^{\boldsymbol{\ell}}\right)^j \left(1 - P_D^{\boldsymbol{\ell}}\right)^{N-j} \tag{8}$$

In the proposed processing scheme, a multistatic data combination in square amplitudes is implemented before thresholding. Let $\{\boldsymbol{\ell}_1, \ldots, \boldsymbol{\ell}_N\}$ be the set of cells of the N bistatic maps where the hypothesised target is located and let $\boldsymbol{m}$ be the cell of the multistatic map corresponding to the best energy alignment, namely $\boldsymbol{m} = \sum_i |\boldsymbol{\ell}_i|^2$. To derive the probability of false alarm $P_{FA}^{\boldsymbol{m}}$ and the probability of detection $P_{D+L}^{\boldsymbol{m}}$ of the proposed scheme, the probability density function under the null and alternative hypothesis, $p_{\mathcal{M}}(\boldsymbol{m};\mathcal{H}_0)$ and $p_{\mathcal{M}}(\boldsymbol{m};\mathcal{H}_1)$, respectively, need to be evaluated.

From the assumed statistical model, $p_{\mathcal{M}}(\boldsymbol{m};\mathcal{H}_0)$ follows a Gamma distribution with shape parameter N and scale parameter P_w. Therefore, the probability of false alarm is given by

$$P_{FA}^{\boldsymbol{m}} = 1 - \gamma\left(N, \eta^{\boldsymbol{m}}/P_w\right) \Big/ \Gamma(N) \tag{9}$$

$$\begin{aligned} p_{\mathcal{M}}(\boldsymbol{m};\mathcal{H}_1) = {} & \frac{1}{P_w} \prod_{i=1}^{N} \frac{1}{1+SNR_i} \\ & \cdot \sum_{j=1}^{N} \frac{e^{-\boldsymbol{m}/P_w\left(1+SNR_j\right)}}{\prod_{\substack{k=1 \\ k\neq j}}^{N} \left(\frac{1}{1+SNR_k} - \frac{1}{1+SNR_j}\right)}, SNR_j \\ & \neq SNR_k\ (j,k = 1,\ldots,N) \end{aligned} \tag{10}$$

$$\begin{aligned} P_{D+L}^{\boldsymbol{m}} = {} & \prod_{i=1}^{N} \frac{1}{1+SNR_i} \\ & \cdot \sum_{j=1}^{N} \frac{\left(1+SNR_j\right) e^{-\frac{\eta^{\boldsymbol{m}}/P_w}{SNR_j+1}}}{\prod_{\substack{k=1 \\ k\neq j}}^{N} \left(\frac{1}{1+SNR_k} - \frac{1}{1+SNR_j}\right)}, SNR_j \\ & \neq SNR_k\ (j,k = 1,\ldots,N) \end{aligned} \tag{11}$$

where $\Gamma(\cdot)$ is the Gamma function, $\gamma(a,b) = \int_0^b t^{a-1}e^{-t}dt$ is the lower incomplete gamma function, and $\eta^{\boldsymbol{m}}$ is the detection threshold.

Under the alternative hypothesis, $\boldsymbol{m}$ is the result of the summation of N independent negative exponential distributions with different rate parameters [22]. Therefore, $p_{\mathcal{M}}(\boldsymbol{m};\mathcal{H}_1)$ is given by (10) and the probability of detection is consequently obtained as (11). It has to be underlined that in (11), strictly different SNRs among the bistatic channels are assumed. In the special case $SNR_i = SNR\ \forall\, i$, $\boldsymbol{m}$ is the result of the summation of N independent negative exponential distributions with same rate parameters and therefore $p_{\mathcal{M}}(\boldsymbol{m};\mathcal{H}_1)$ follows a Gamma distribution with shape parameter N and scale parameter $P_w(1+SNR)$. Therefore, under these special conditions,

$$P_{D+L}^{\boldsymbol{m}} = 1 - \gamma\left(N, \eta^{\boldsymbol{m}}/P_w(1+SNR)\right) \Big/ \Gamma(N) \tag{12}$$

We point out that, as with the proposed scheme the target Cartesian position is provided jointly with its detection, (11) and (12) also represent the probability of localisation, which has been denoted with the subscript $D+L$.

3.2 | Numerical analysis

Let σ_i be the bistatic RCS of the target illuminated by the i th satellite. The SNR available in map $\mathcal{B}_i$ can be expressed as

$$SNR_i = \frac{P_{DenGr} G \lambda^2 T_a \sigma_i}{(4\pi)^2 d^2 k_B T_0 F L_s} \tag{13}$$

where $d = \|\boldsymbol{p}\|$ is the target to receiver distance, P_{DenGr} is the flux power density of the GNSS transmission on the Earth surface, G is the gain of the surveillance channel antenna, F is the noise figure and T_0 is the noise temperature, k_B is the Boltzmann constant and L_s denotes system losses. Table 1 lists the parameters assumed in the remainder of the section, which

TABLE 1 Link budget parameters.

Parameter		Value
Satellite illuminators	Constellation	Galileo
	Band	E5a
	Carrier frequency	1176.45 MHz
	Power density on the ground	−135 dBW/m^2
Receiver and processing	Radar antenna gain	15 dB
	Noise figure	1.5 dB
	Noise temperature	290 K
	System losses	2 dB
	Coherent processing interval	3 s

are compliant with the experimental campaigns detailed in Section 4.

In a first analysis, we assume a target characterised by an RCS independent of the particular transmitter viewing angle, namely same SNR in the N bistatic channels. Figure 3 shows the detection and localisation performance of the conventional and the proposed schemes for different values of the SNR characterising the individual RD maps and for a small ($N = 3$) and a large ($N = 10$) number of used satellites. For both the techniques, thresholds have been selected to guarantee a false alarm rate equal to 0.001. Full lines represent the theoretical performance, while the markers show the simulated results obtained via Monte Carlo simulations (10,000 independent trials for each data point). Black and pink curves show the detection and localisation performance, respectively, of the conventional approach, that is, $P_D^{\phi} i = P_D^{\phi}$ and P_L^{ϕ}, while the probabilities of joint detection and localisation P_{D+L}^{m} achievable with the proposed strategy are represented by the blue curves. As it is apparent, the proposed approach can significantly outperform the conventional scheme. For example, for a ship target characterised by RCS $\sigma = 300$ m^2 (which could likely correspond to a small coaster) sailing at distance $d = 3$ km from the receiver, resulting in $SNR \approx 8$ dB in each bistatic map, P_L^{ϕ} is about 39% only when three satellites are available, while P_{D+L}^{m} reaches 80%.

Figure 4 shows the maximum radar range d_{max} as a function of the number of available satellites. The bistatic RCS has been set in each bistatic channel equal to 1000 m^2 (that could correspond to a medium size coaster) and user requirements for evaluating d_{max} are localisation probability better than 75% for false alarm rate not exceeding 10^{-3}. From the figure, it can be seen as when the minimum number of satellites $N = 2$ is used, the target can be reliably detected and localised at a range of not more than 2 km with the conventional approach, while it extends up to ~5 km with the proposed strategy. Using Equations (8) and (12), it is easy to verify that this corresponds to a SNR gain of about 7.5 dB moving from the conventional to the proposed approach, which therefore allows reaching the same maximum radar range for considerably smaller targets. Actually, the performances of both the schemes significantly improve for larger N values, however, the proposed strategy always outperforms the conventional technique, enabling surveying larger areas/smaller ships in parity of exploited satellites.

So far, we analysed the system performance under the simplified assumption of ship RCS independent of the illumination angle. However, in real scenarios, the different bistatic angles due to the different satellites' positions combined with the complex shape of ship targets make the RCS to vary with the particular satellite, so that different SNRs among the multiple bistatic channels are experienced. To investigate the techniques performance under these conditions, we assume the target to be characterised by an average RCS $\overline{\sigma}$ and the ith bistatic RCS is given by $\sigma_i = a_i \overline{\sigma}$, where a_i are weighting coefficients such that $\sum_i a_i = N$. Figure 5 shows the theoretical (full and dotted lines) and simulated (markers) detection and localisation probabilities of the conventional and proposed approaches for a target located at $d = 3$ km from the receiver and $N = 3$ satellites. In Figure 5a, a smooth variation of the RCS with the bistatic geometry has been considered ($a_1 = 0.8$, $a_1 = 1$ and $a_3 = 1.2$). The superior performance of the proposed scheme can be appreciated: for example, for $\overline{\sigma} \approx 400$ m^2, the detection probabilities on the individual bistatic channels (dotted lines) are about 40%–50%, bringing to $P_L^{\phi} \cong 50\%$; in contrast, with the proposed procedure, such a ship can be detected and jointly localised with a probability of about 90%. In a second case study, Figure 5b, a significant RCS scintillation has been considered by setting $a_1 = a_2 = 0.2$ and $a_3 = 2.6$, in order to simulate the scenario where a particular satellite provides a much stronger reflected signal than others. In this scenario, localisation performance of the conventional method are significantly compromised by the low detection

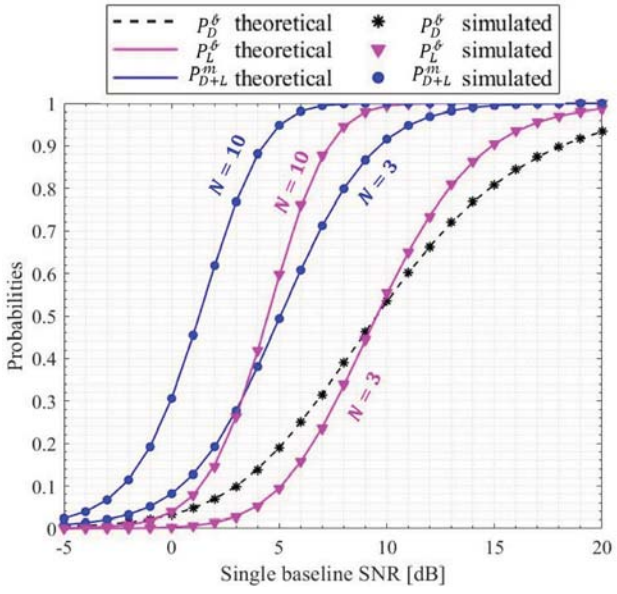

FIGURE 3 Detection and localisation performance.

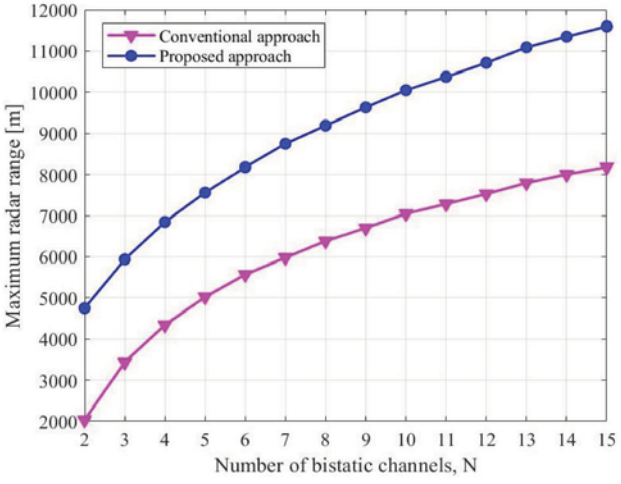

FIGURE 4 Maximum radar range versus number of available satellites for ship radar cross section (RCS) $\sigma = 1000$ m^2.

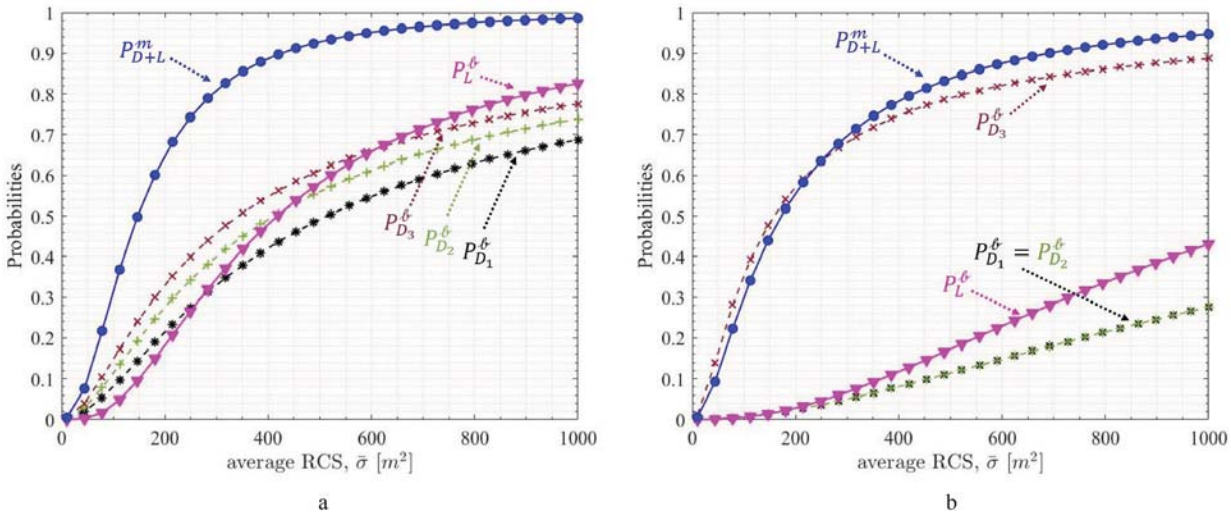

FIGURE 5 Probability of detection and localisation as a function of the average radar cross section (RCS) for smooth (a) and strong (b) RCS scintillation.

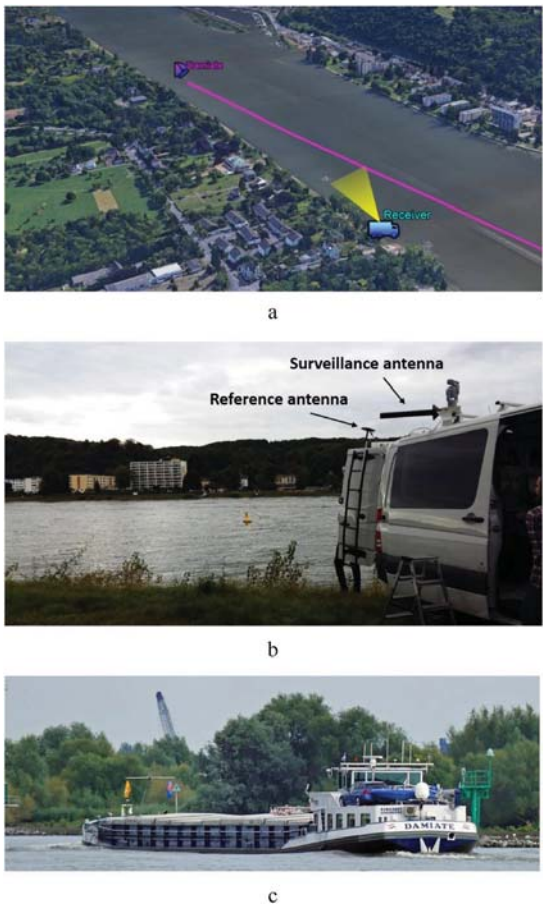

FIGURE 6 Experimental trials on the Rhine – (a) Acquisition geometry, (b) passive receiver, and (c) *Damiate* photograph.

performance of channels 1 and 2, because of the large probability that the target is detected in $\mathcal{B}_3$ only, while, thanks to the combination in square amplitudes, the proposed approach provides much higher localisation probabilities.

TABLE 2 Rhine river experimental trials.

Parameter		Value
Satellite 1	Number	GSAT0208
	PRN	E08
	Aspect angle*	−123.7°
	Elevation angle	25.7°
Satellite 2	Number	GSAT0205
	PRN	E24
	Aspect angle	153.4°
	Elevation angle	12.2°
Ship	Name	Damiate
	MMSI	244700319
	Type	Inland motor freighter
	Size	85 m × 8.3 m

Abbreviations: PRN, Pseudo random noise; MMSI, Maritime mobile service identity.
*clockwise from the X-axis.

4 | EXPERIMENTAL RESULTS

Experiments have been conducted in different scenarios of practical interest. The experimental hardware was a superheterodyne receiver mounted onto a van collecting signals transmitted by Galileo satellites in the E5a band, broadcasting PRN codes with chip-rates equal to 10.23 MHz. The receiving station was also equipped with an Automatic Identification System (AIS) receiver to record in real time the ship actual location to be used as ground truth. Optical photographs and ancillary information of the ships of opportunity exploited in the experiments have been obtained from [23] by reading the Maritime Mobile Service Identity (MMSI) number from the AIS data log. In all the experiments, T_a has been set equal to 3 s.

4.1 | River traffic monitoring

In the first scenario, the passive radar prototype was placed on the bank of the Rhine near Bonn, Germany, observing the river traffic. Figure 6a shows the acquisition geometry, while a photograph of the receiver is shown in Figure 6b. During the acquisition, the inland motor freighter *Damiate*, shown in Figure 6c, was in the radar antenna field of view, moving away from the receiver. Two Galileo satellites were correctly acquired by the reference channel, whose parameters are listed in Table 2.

Figure 7 shows the RD maps $\mathcal{B}_1$ and $\mathcal{B}_2$ corresponding to satellites GSAT0208 and GSAT0205, respectively, centred in the target position and where 0 dB denotes the mean background power. As in this case the ship was at a very short receiver standoff (less than 500 m), a quite well visible intensity peak can be observed in both the maps, in positions that could be shown being very close to the range and Doppler positions retrieved from the AIS. Particularly, SNRs equal to about 13 dB in $\mathcal{B}_1$ and about 14 dB in $\mathcal{B}_2$ have been obtained. By setting $P_{FA}^{\phi} = 10^{-3}$, these values correspond to quite high peripheral detection probabilities: from (6), $P_{D_1}^{\phi} \approx 77\%$ and $P_{D_2}^{\phi} \approx 81\%$. Nevertheless, as in this case study only two satellites were tracked from the reference channel, successful localisation requires the target to be detected in both the maps. Namely, the localisation probability of the conventional approach (7) here reduces at the products of the detection probabilities of the two RD maps, that is, $P_L^{\phi} \approx 62\%$, which could not suffice, for example, in case of waterways subject to dense traffic. In contrast, with the proposed technique, the multistatic integration gain allows to achieve a probability of detection and localisation $P_{D+L}^{\mathcal{M}}$ better than 93%. Noticeably, to achieve the

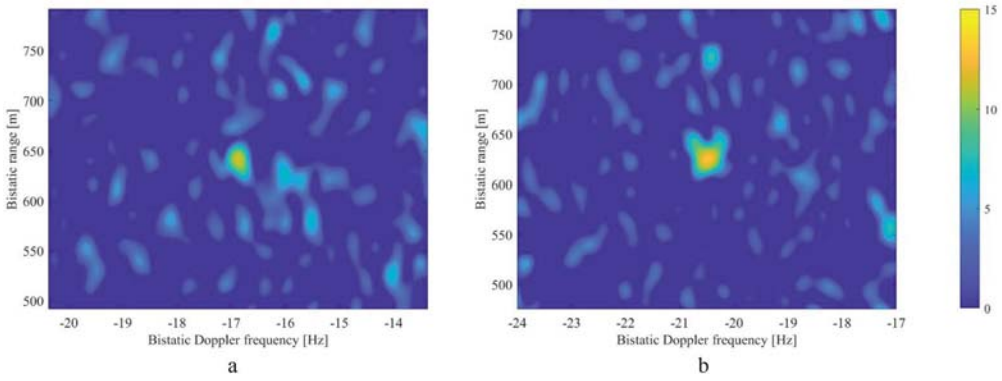

FIGURE 7 Damiate – experimental Range and Doppler (RD) maps. (a) $\mathcal{B}_1$ and (b) $\mathcal{B}_2$.

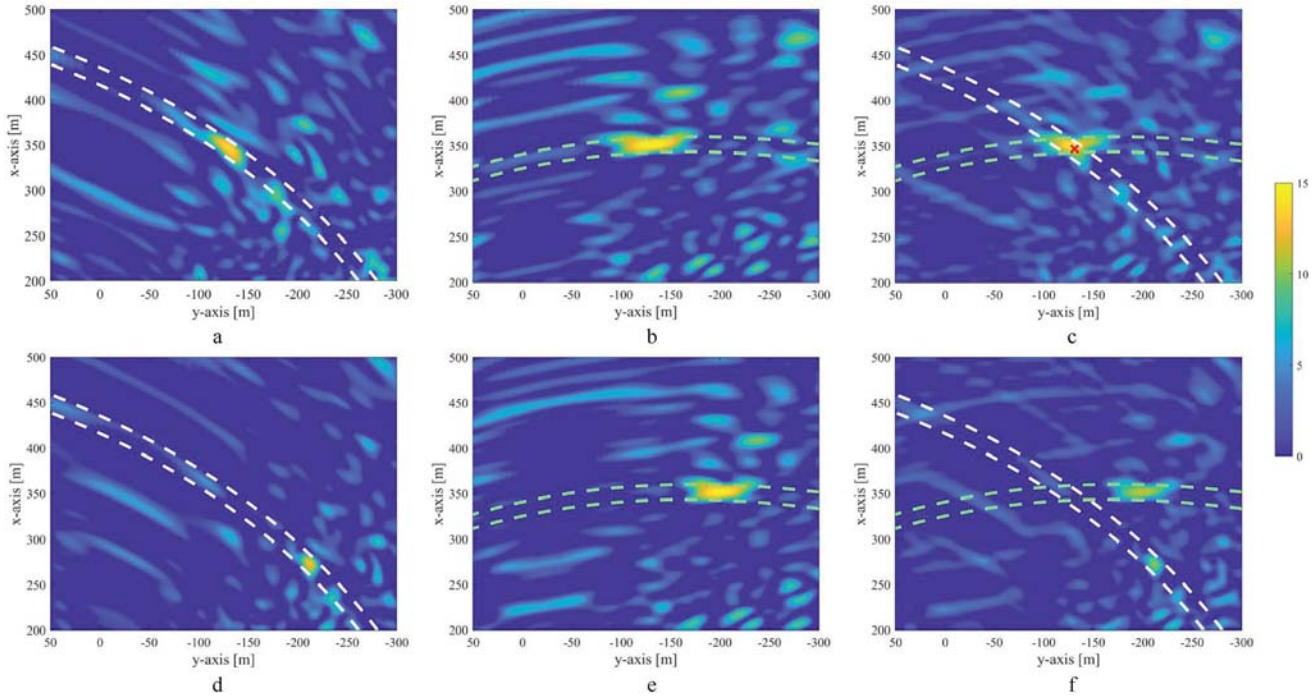

FIGURE 8 Damiate – experimental $\mathcal{M}_i$ and $\mathcal{M}$ maps for different tested velocities - (a) $\mathcal{M}_1(x, y; \boldsymbol{v}_1)$, (b) $\mathcal{M}_2(x, y; \boldsymbol{v}_1)$, (c) $\mathcal{M}(x, y; \boldsymbol{v}_1)$, (d) $\mathcal{M}_1(x, y; \boldsymbol{v}_2)$, (e) $\mathcal{M}_2(x, y; \boldsymbol{v}_2)$, and (f) $\mathcal{M}(x, y; \boldsymbol{v}_2)$.

FIGURE 9 Experimental trials at the Venice lagoon. (a) Surveyed area and (b) *Metamauco* photograph.

TABLE 3 Venice lagoon experimental trials.

Parameter		Value
Satellite 1	Number	GSAT0214
	PRN	E05
	Aspect angle	172.5°
	Elevation angle	55.1°
Satellite 2	Number	GSAT0205
	PRN	E24
	Aspect angle	168.5°
	Elevation angle	42.7°
Ship	Name	Metamauco
	MMSI	247290200
	Type	Ro-ro
	Size	57.85 m × 13.1 m

Abbreviation: MMSI, Maritime mobile service identity.

same probability of localisation with the conventional approach (assuming same SNR among the baselines), a SNR ~10 dB higher would be required.

It is worth to notice that the maximum integration gain is obtained when the target power observed in the individual bistatic channels is mapped around the same position in the single satellite maps. For sake of illustration, Figure 8 shows maps $\mathcal{M}_1$ and $\mathcal{M}_2$ corresponding to the two bistatic geometries and the corresponding multistatic maps when velocities $\boldsymbol{v}_1 = [2.9, -0.1]$ m/s (corresponding to the value provided by the AIS) and $\boldsymbol{v}_2 = [3, -0.3]$ m/s are used in the $\mathcal{B}_i$ to $\mathcal{M}_i$ mapping. Figure 8a–c correspond to the maps achieved using the actual target velocity $\boldsymbol{v}_1$, while results achieved with $\boldsymbol{v}_2$ are shown in Figure 8d–f. The dashed lines superimposed to the figures are the iso-ranges (one resolution cell) corresponding to GSAT0208 (white lines) and GSAT0205 (green lines). Comparing the maps pertaining the same satellite but using different velocity in the mapping, it can be observed as the target energy moves along iso-range contours, concentrating around the target real position [red '×' marker in Figure 8c] when the actual velocity is used. Under such conditions, the best alignment among the N $\mathcal{M}_i$ maps is achieved, thus maximising the integration gain.

4.2 | Inland passenger water transport control

The second acquisition campaign was carried out at the Venice Lagoon, Italy, with the receiver installed on the West side of the Venice Lido Island with the surveillance antenna pointed towards the waterway crossing the lagoon (distance from the shores ~ 1 km), mainly populated by water buses and cruise ships. Figure 9a and b shows a photograph of the surveyed area and the ro-ro passenger car ferry *Metamauco*, which was headed towards the Giudecca Canal.

Table 3 lists the parameters of the two exploited satellites and the opportunistic target, while Figure 10 shows the achieved RD maps, also in this case normalised to the mean background power. From the white boxes in the top right corners showing the zooms around the target position, it can

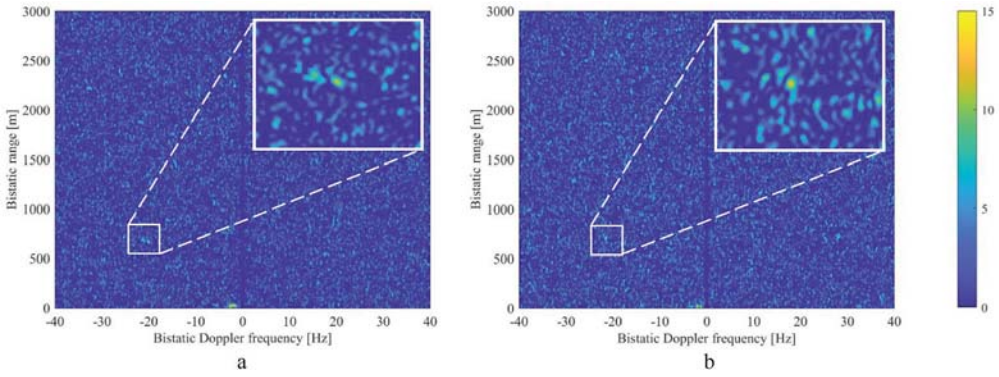

FIGURE 10 *Metamauco* experimental Range and Doppler (RD) maps. (a) $\mathcal{B}_1$ and (b) $\mathcal{B}_2$.

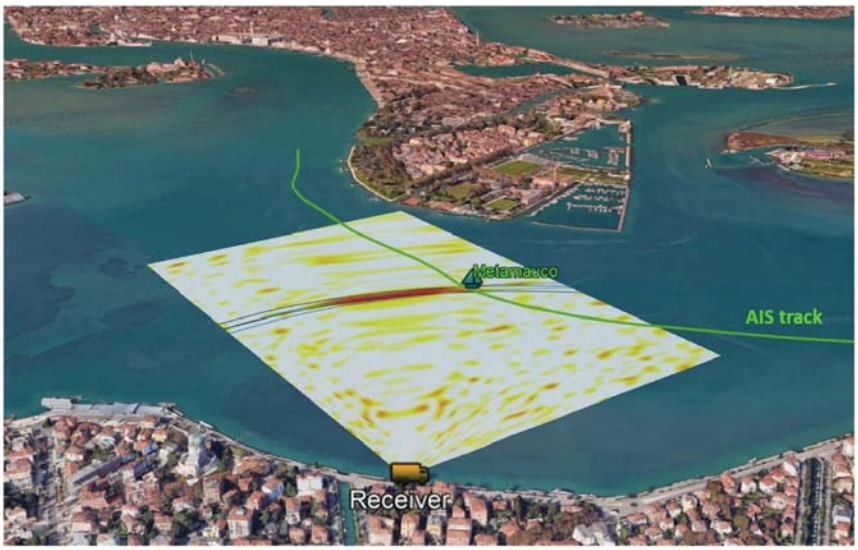

FIGURE 11 Venice lagoon - experimental multistatic map $\mathcal{M}$ superimposed to the surveyed area.

FIGURE 12 Experimental trials at the Marghera Port - (a) System geometry and (b) *Fairpartner* photograph.

be seen as the target is hardly detectable in both the individual bistatic channels, carrying to limited chances to localise it with the conventional two-stage strategy (from the measured SNRs, $P^{\phi}_{D_1} \approx 47\%$ and $P^{\phi}_{D_2} \approx 56\%$ so that $P^{\phi}_{L} \approx 26\%$ when $P^{\phi}_{FA} = 10^{-3}$).

Figure 11 shows the multistatic map corresponding to the velocity providing the highest integration gain georeferenced and superimposed to the optical image of the acquisition area. It can be observed as in the map a bright area can be identified, thus giving rise to a high probability of detection. Particularly, the integrated SNR allows to have $P^{\mathcal{M}}_{D+L} \approx 87\%$, that is, the probability to detect the ship with the proposed approach is

TABLE 4 Marghera Port experimental trials.

Parameter		Value
Satellite 1	Number	GSAT0206
	PRN	E30
	Aspect angle	159.4°
	Elevation angle	49.9°
Satellite 2	Number	GSAT0207
	PRN	E07
	Aspect angle	−51.8°
	Elevation angle	65.8°
Satellite 3	Number	GSAT0211
	PRN	E02
	Aspect angle	66.8°
	Elevation angle	49.2°
Satellite 4	Number	GSAT0208
	PRN	E08
	Aspect angle	102.1°
	Elevation angle	56.1°
Ship	Name	Fairpartner
	MMSI	246467000
	Type	Heavy load carrier
	Size	143.1 m × 26 m

Abbreviations: PRN, pseudo random noise; MMSI, Maritime mobile service identity.

~40% and ~31% higher than with the individual maps $\mathcal{B}_1$ and $\mathcal{B}_2$, respectively, while the chance to localise it is increased of ~60%, corresponding to a SNR gain of about 8.5 dB. Nevertheless, inspecting the figure, it can be observed as the bright return corresponding to the target spans over a quite large area, so that a poor localisation accuracy can be expected,

as it is also confirmed comparing the location of the bright area with the AIS position. Such a behaviour is due to the orientation of the two bistatic iso-ranges, depicted by blue and black dotted lines in the figure. Particularly, it is possible to see as both the bistatic geometries provided very close iso-ranges, thus entailing a large overlapping area. Obviously, increasing the number of satellites can allow overcoming such an unfavourable situation.

4.3 | Support to port operations

A further acquisition took place at Marghera Port, Italy. The receiver was located at the entrance of the harbour, observing the vessels along the waterway access to the port, as shown in Figure 12a. During the acquisition, the cargo *Fairpartner* [Figure 12b], was inside the receiver field of view while it was headed towards the port terminals at about 1.2 km distance. In this case, four Galileo satellites were correctly tracked, giving us the chance to have at our disposal multiple bistatic channels significantly separated in angle, as shown in Table 4.

Figure 13 shows the individual RD maps corresponding to the time instant at the beginning of the acquisition, where the top-right white corners show the zooms around the target position according to the AIS information. It can be observed as the different illumination angles bring to a large variation of the received target power. Particularly, sat. 1 provides a SNR level significantly high, with a peak power of about 30 dB above the mean disturbance level, while the target is barely visible when illuminated by the other satellites, with a very poor observability in the case of sat. 4. These experimental results strongly encourage to opt for integration over multiple bistatic geometries rather than over multiple frames as a mean to increase the target observability in the GNSS-based passive radar, due to the higher chances to intercept an illumination angle providing a high bistatic RCS.

To verify the potentialities of the proposed approach under challenging conditions, hereinafter we assume that sat. 1 was not available. First, Table 5 lists the detection and localisation probabilities resulting from the measured SNRs for the considered time instant when the false alarm rate has been set equal to 10^{-3} and 10^{-4}, showing as the proposed approach may enable reliable target detection and localisation even for lower values of the false alarm rate, while the conventional

TABLE 5 Fairpartner experimental probabilities of detection and localisation.

$P^{\phi}_{FA}, P^{m}_{FA}$	$P^{\phi}_{D_2}$	$P^{\phi}_{D_3}$	$P^{\phi}_{D_4}$	P^{ϕ}_{L}	P^{m}_{D+L}
10^{-3}	69.89%	62.06%	51.34%	66.58%	95.50%
10^{-4}	62.02%	52.94%	41.11%	53.10%	92.51%

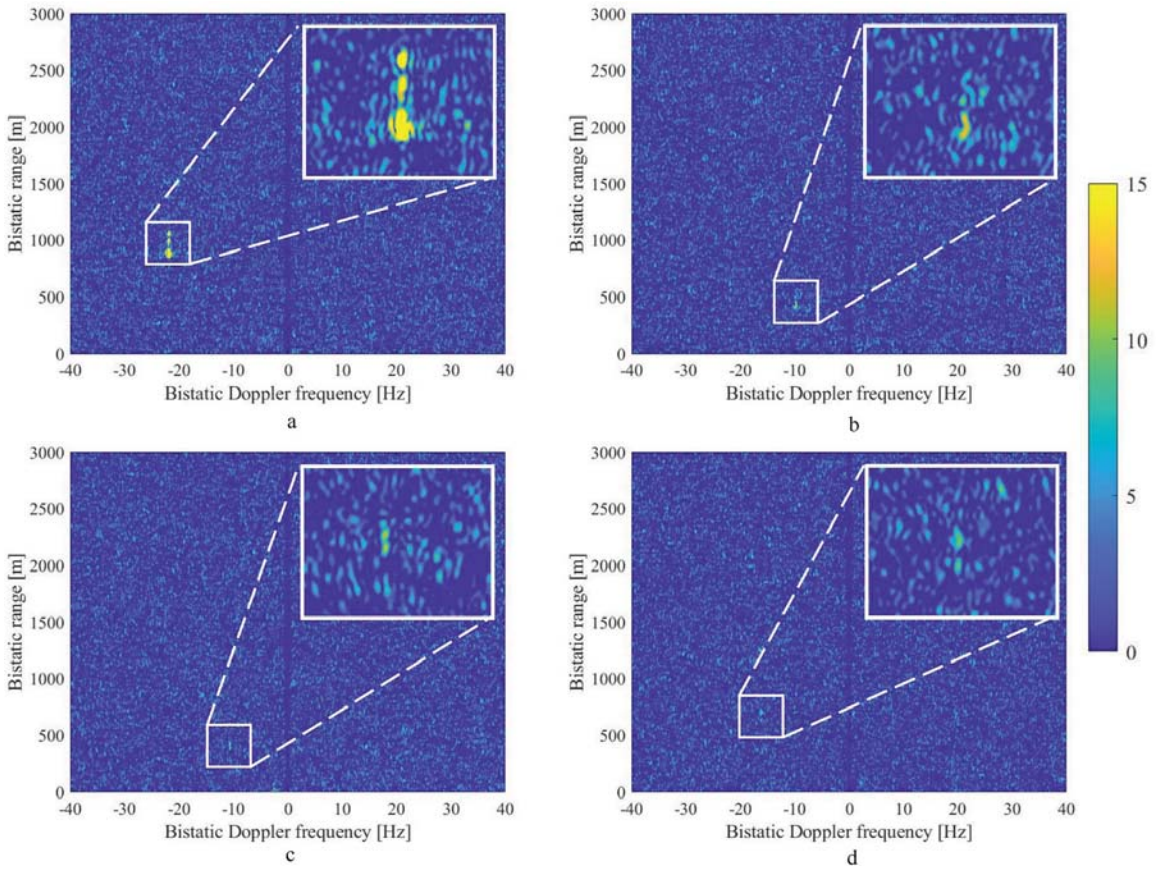

FIGURE 13 Fairpartner bistatic Range and Doppler (RD) maps - (a) sat. 1, (b) sat. 2, (c) sat. 3, and (d) sat. 4.

approach provides poor performance, due to the high missed detection rates in the individual channels. Moreover, it is worth to note that for the bistatic channel observing the lowest SNR (sat. 4), reinforcing the target power by multi-frame integration procedures as in [7–11] would not suffice to achieve the same detection performance of the proposed approach. Indeed, from the statistical model in Section 3.1, it could be easily shown that by integrating $N_f = 3$ frames (assuming an ideal motion compensation) pertaining sat. 4 only would bring to a bistatic detection probability of about 80% (false alarm rate 10^{-3}), that is, lower than the detection probability achievable with the proposed method using one single frame and $N = 3$ satellites. Moreover, the exploitation of multiple satellites in lieu of multiple frames has the further advantage of a direct target localisation, whose performance in this case study are addressed below.

The localisation performance have been tested for the whole target trajectory. Particularly, the conventional bistatic detections then localisation and the proposed multistatic joint detection and localisation approaches have been applied to successive CPIs by shifting each time the starting time of 5 s, for a total of 21 timestamps. Figure 14 shows the estimated positions (on the Cartesian and on the georeferenced plane) over the target trajectory. For both the methods, the target RD/Cartesian position is obtained as central position of the cluster of pixels of the corresponding binary maps after thresholding according to Equations (5) and (9) (false alarm rate equal to 0.001) followed by clustering. Figure 14a and b refer to the conventional approach, while the results with the proposed method are shown in Figure 14c and d. In the conventional approach, in a few instants the target has been detected on a single channel. Therefore, in such cases, a missed localisation event occurs, which has been indicated with a '◊' marker in the figure. Table 6 lists the successful ('✓') and missed ('×') localisations for each timestamp. We can observe as with the conventional and proposed approaches the target has been localised in 12 out of 21 and 21 out of 21 instants, respectively, corresponding to estimated $P_L^{\prime}$ of about 57% and $P_{D+L}^{\prime\prime\prime}$ of 100% (therefore in line with the theoretical expectations reported in Table 5).

Moreover, comparing the estimated tracks, the lower dispersion of the estimates with the proposed approach can be easily appreciated. Particularly, as reported in the last row of Table 6, the proposed approach provides a root mean square (RMS) error (evaluated by taking the AIS positions as reference) of about 40 m, therefore one hundred metres better than the conventional approach and even better that the target length.

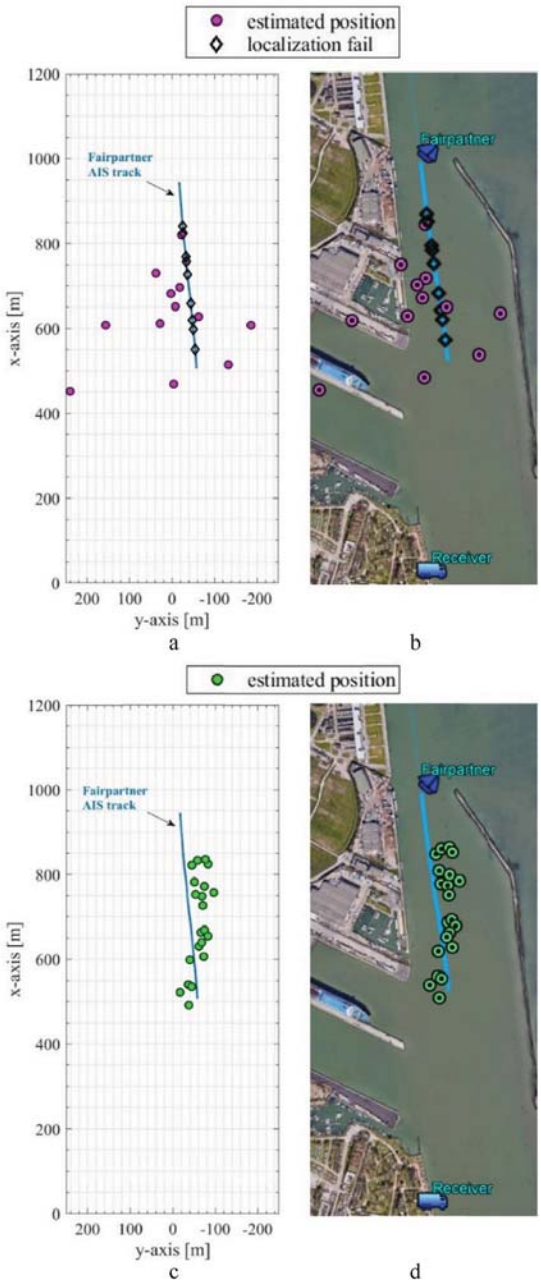

FIGURE 14 *Fairpartner* estimated positions - conventional bistatic detection than localisation: (a) Cartesian plane, (b) georeferenced plane; proposed multistatic joint detection and localisation: (c) Cartesian plane, (d) georeferenced plane.

5 | CONCLUSION

In this work, a novel approach for ship detection and localisation with a multistatic radar systems based on GNSS illuminators has been introduced. Particularly, the proposed scheme capitalises on the spatial diversity provided by navigation satellites to overcome the limitations posed by the restricted power budget of the system. The proposed procedure projects the data pertaining the multiple bistatic geometries over a common reference plane, allowing to reinforce the received target power by means of non-coherent integration on a pixel basis. As the procedures entirely operates on the Cartesian plane, it can provide a clear picture of the surveyed area, providing in a single step the target detection and its position within the surveyed area. The method can benefit of a shorter dwell than other approaches recently developed for this type of radar systems, enhancing its resilience against motion model mismatches, typically affecting conventional long integration time strategies.

TABLE 6 Fairpartner localisation results.

CPI starting instant [s]	Bistatic detection then localisation	Multistatic joint detection and localisation
0	✓	✓
4	✓	✓
9	✓	✓
14	×	✓
19	✓	✓
24	×	✓
29	✓	✓
34	×	✓
39	✓	✓
44	×	✓
49	✓	✓
54	✓	✓
59	✓	✓
64	×	✓
69	✓	✓
74	×	✓
79	×	✓
84	✓	✓
89	✓	✓
94	×	✓
99	×	✓
Tot	12/21 → 57%	21/21 → 100%
RMS error	143 m	40 m

Abbreviation: CPI, Coherent processing interval; RMS, Root mean square.

Detection and localisation capability and corresponding maximum radar range have been evaluated at the theoretical level, comparing the performance with those achievable when conventional bistatic detections then localisation procedures are applied. Then, the effectiveness of the approach has been tested in a number of experimental case studies, including different scenarios and ships belonging to different types/dimensional classes. The achieved results showed as the proposed approach can outperform conventional two stages procedures in different situations of practical interest.

Finally, it is worth to point out that the proposed approach can be immediately extended to the multiple frequency case, as the RD data are projected in a domain independent, as well as from the satellite position, from the carrier frequency. Actually, GNSS operate on multiple frequency channels in the L-band, and new channels could become available in the future in the C-band and/or the S-band. As man-made targets like ships are quite sensitive to small changes of the wavelength of the impinging signals, the exploitation of multiple frequency channels could give rise to a significant variation of the target RCS, that could be exploited to further increase the system performance.

AUTHOR CONTRIBUTION

Ilaria Nasso: conceptualisation, investigation, writing original draft. **Fabrizio Santi:** conceptualisation, supervision, writing review and editing.

ACKNOWLEDGEMENTS

The experimental campaigns were carried out inside the research project "GALILEO-BASED PASSIVE RADAR SYSTEM FOR MARITIME SURVEILLANCE—SpyGLASS" funded from the European GNSS Agency under the European Union's Horizon 2020 research and innovation programme under grant agreement No. 641486.

CONFLICT OF INTEREST STATEMENT

The authors declare no conflict of interest.

DATA AVAILABILITY STATEMENT

Research data are not shared.

ORCID

Ilaria Nasso https://orcid.org/0000-0002-5090-5663
Fabrizio Santi https://orcid.org/0000-0003-3039-1690

REFERENCES

1. Stove, A.G., et al.: Passive maritime surveillance using satellite communication signals. IEEE Trans. Aero. Electron. Syst. 53(6), 2987–2997 (2017). https://doi.org/10.1109/taes.2017.2722598
2. Daniel, L., et al.: Design and validation of a passive radar concept for ship detection using communication satellite signals. IEEE Trans. Aero. Electron. Syst. 53(6), 3115–3134 (2017). https://doi.org/10.1109/taes.2017.2728978
3. Golabi, M., Sheikhi, A., Biguesh, M.: A new approach for sea target detection in satellite based passive radar. In: 2013 21st Iranian Conference on Electrical Engineering (ICEE), Mashhad, Iran, pp. 1–5 (2013)
4. Pisciottano, I., Cristallini, D., Pastina, D.: Maritime target imaging via simultaneous DVB-T and DVB-S passive ISAR. IET Radar, Sonar Navig. 13(9), 1479–1487 (2019). https://doi.org/10.1049/iet-rsn.2018.5622
5. Ma, H., et al.: Maritime moving target indication using passive GNSS-based bistatic radar. IEEE Trans. Aero. Electron. Syst. 54(1), 115–130 (2018). https://doi.org/10.1109/taes.2017.2739900
6. Gomez-Del-Hoyo, P., Gronowski, K., Samczynski, P.: The STARLINK-based passive radar: preliminary study and first illuminator signal measurements. In: 2022 23rd International Radar Symposium (IRS), Gdansk, Poland, pp. 350–355 (2022)
7. Pastina, D., et al.: Maritime moving target long time integration for GNSS-based passive bistatic radar. IEEE Trans. Aero. Electron. Syst. 54(6), 3060–3083 (2018). https://doi.org/10.1109/taes.2018.2840298
8. Pieralice, F., et al.: GNSS-based passive radar for maritime surveillance: long integration time MTI technique. In: 2017 IEEE Radar Conference (RadarConf), Seattle, WA, USA, pp. 0508–0513 (2017)
9. Li, Z., et al.: Multi-frame fractional Fourier transform technique for moving target detection with space-based passive radar. IET Radar, Sonar Navig. 11(5), 822–828 (2017). https://doi.org/10.1049/iet-rsn.2016.0432
10. Huang, C., et al.: BeiDou-based passive radar vessel target detection: method and experiment via long-time optimized integration. Rem. Sens. 13(19), 3933 (2021). https://doi.org/10.3390/rs13193933

11. He, Z., Yang, Y., Chen, W.: A hybrid integration method for moving target detection with GNSS-based passive radar. IEEE J. Sel. Top. Appl. Earth Obs. Rem. Sens. 14, 1184–1193 (2021). https://doi.org/10.1109/jstars.2020.3037200
12. Santi, F., Pieralice, F., Pastina, D.: Joint detection and localization of vessels at sea with a GNSS-based multistatic radar. IEEE Trans. Geosci. Rem. Sens. 57(8), 5894–5913 (2019). https://doi.org/10.1109/tgrs.2019.2902938
13. Santi, F., Pastina, D., Bucciarelli, M.: Experimental demonstration of ship target detection in GNSS-based passive radar combining target motion compensation and track-before-detect strategies. Sensors 20(3), 599 (2020). https://doi.org/10.3390/s20030599
14. Li, Z., et al.: BeiDou-based passive multistatic radar maritime moving target detection technique via space-time hybrid integration processing. IEEE Trans. Geosci. Rem. Sens. 60, 1–13 (2022). https://doi.org/10.1109/tgrs.2021.3128650
15. Nasso, I., Santi, F.: A centralized ship localization strategy for passive multistatic radar based on navigation satellites. Geosci. Rem. Sens. Lett. IEEE 10, 1–5 (2022). https://doi.org/10.1109/lgrs.2022.3204169
16. Ma, H., et al.: Maritime moving target localization using passive GNSS-based multistatic radar. IEEE Trans. Geosci. Rem. Sens. 56(8), 4808–4819 (2018). https://doi.org/10.1109/tgrs.2018.2838682
17. Sadeghi, M., Behnia, F., Amiri, R.: Maritime target localization from bistatic range measurements in space-based passive radar. IEEE Trans. Instrum. Meas. 70, 1–8 (2021). https://doi.org/10.1109/tim.2021.3076584
18. Nasso, I., Santi, F.: A Centralized Approach for Ship Target Detection and Localization with Multi-Transmitters GNSS-Based Passive Radar. IET International Conf. Radar Syst., Edinburgh (2022)
19. Bar-Shalom, O., Weiss, A.J.: Direct positioning of stationary targets using MIMO radar. Signal Process. 91(10), 2345–2358 (2011). https://doi.org/10.1016/j.sigpro.2011.04.019
20. Yi, W., et al.: Suboptimal low complexity joint multi-target detection and localization for non-coherent MIMO radar with widely separated antennas. IEEE Trans. Signal Process. 68, 901–916 (2020). https://doi.org/10.1109/tsp.2020.2968282
21. Wang, Y.H.: On the number of successes in independent trials. Stat. Sin. 3(2), 295–312 (1993)
22. Levy, E.: On the density for sums of independent exponential, Erlang and gamma variates. Stat. Pap. 63(3), 1–29 (2021). https://doi.org/10.1007/s00362-021-01256-x
23. 'Marine traffic'. Accessed 26/12/2022 [Online]. https://www.marinetraffic.com

How to cite this article: Nasso, I., Santi, F.: Maritime moving target detection and localisation technique for Global Navigation Satellite Signals-based passive multistatic radar. IET Radar Sonar Navig. 1–14 (2023). https://doi.org/10.1049/rsn2.12438